

Left-ventricle myocardium segmentation using a coupled level-set with a priori knowledge

M. Lynch*, O. Ghita, P.F. Whelan

Vision Systems Group, Dublin City University, Dublin 9, Ireland

Received 15 July 2005; received in revised form 17 November 2005; accepted 28 March 2006

Abstract

This paper presents a coupled level-set segmentation of the myocardium of the left ventricle of the heart using a priori information. From a fast marching initialisation, two fronts representing the endocardium and epicardium boundaries of the left ventricle are evolved as the zero level-set of a higher dimension function. We introduce a novel and robust stopping term using both gradient and region-based information. The segmentation is supervised both with a coupling function and using a probabilistic model built from training instances. The robustness of the segmentation scheme is evaluated by performing a segmentation on four unseen data-sets containing high variation and the performance of the segmentation is quantitatively assessed.

© 2006 Elsevier Ltd. All rights reserved.

Keywords: Level-set; Segmentation; Cardiac; Left-ventricle; Coupled; A priori knowledge

1. Introduction

Early identification of myocardium dysfunction through quantitative analysis, permits a reliable and fast diagnosis of heart diseases. Such quantitative functions include left ventricle ejection fraction, left ventricle myocardium thickening over the cardiac cycle and left ventricle myocardium mass. To evaluate these measures, accurate delineation of the left ventricle cavity and left ventricle cardiac muscle is required.

Advanced imaging techniques in magnetic resonance imaging (MRI) have allowed for the imaging of the heart muscle at increasing spatial and temporal resolutions. Multisection multiphase short-axis cardiac MR images are the most suitable to assess left ventricle function without drawing any assumptions about left ventricle geometry [1]. Traditional methods of quantitative analysis required the manual delineation of the myocardium. This has become increasingly time consuming with the extra data now available from a single MRI examination. Therefore, an automatic segmentation of the left ventricle myocardium is desired. This issue has been previously addressed in literature and the developed methods can be classified into region-based and boundary finding approaches.

Region-based methods are used to segment the image, commonly using no a priori information. The most basic form of region-based segmentation is thresholding. Thresholding requires a high degree of supervision, high differentiation between the object being segmented and the background and may require some additional post processing. More complex statistical region-based methods like clustering, collect pixels of similar intensities to create a segmentation of structures in the image [2]. However, in some cases the distributions of one structure may locally overlap with those from another structure rendering intensity-based segmentation techniques unusable.

Boundary finding algorithms like snakes [3], aspire to deform a local boundary curve and come to rest on the high frequency data in an image, corresponding to edges. Such algorithms are sensitive to initialisation, local minima and leaking through boundaries of low gradient. The extension of snakes to 3D (active surfaces) has also been applied to cardiac segmentation. Kaus et al. [4], aim to perform an adaption algorithm based on image information and internal constraints using a triangulated surface mesh. An additional coupling constraint is added to the update energies in order to maintain the spatial separation of the inner and outer surface. As this method is derived from snakes, it is sensitive to initialisation and is not applicable to images where the cardiac muscle cannot be represented by a smooth shape.

Active shape models (ASMs) proposed by Cootes et al. [5] use a statistical model built up from a training set of segmented

* Corresponding author. Tel.: +353 1 700 7637.
E-mail address: lynchm@eeng.dcu.ie (M. Lynch).

objects to delineate the desired shape. The model is compiled and then compressed, commonly using principal component analysis (PCA). ASMs have become a prominent tool in the segmentation of the left ventricle [6,7]. It is also worth noting that the accuracy of the segmentation relies heavily on the amount and variation of images in the training set.

Active appearance models (AAMs) [5] are an extension to ASMs which use the texture variation in the training set in the compressed PCA. This method alleviates the problems associated with the ASMs in areas of low gradients. Stegmann and Larsson [8] showed how these active appearance models could be applied to analyse short axis MR images of the heart. Mitchell et al. [9] addresses the problems that AAMs have with attaching the model with the gradient information. A hybrid approach is taken which combines ASMs and AAMs. Lelieveldt and co-workers [10] introduces a time factor into his active appearance motion models (AAMMs) and minimises the appearance-to-target differences.

Level-set methods for segmentation (also called Geodesic Active Contours) were first introduced by Osher and Sethian in 1988 [11] following previous work in Sethian's Ph.D. thesis [12] on flame propagation. The theory behind this boundary-based segmentation is largely based on work in partial differential equations and the propagation of fronts under intrinsic properties such as curvature [13]. The deformation of the level set is seen as a gradient flow to a state of minimal energy providing the object to be segmented has clearly identifiable boundaries [14,15]. By extending the dimensionality of the problem to $N + 1$, where N is the initial dimension of the problem, some advantageous properties can be exploited. These include level-sets ability to deal with local deformations like shape corners, changes in topology and multi-component structures. Such qualities lend themselves well in the field of medical image segmentation where the biological structures split and merge through the volume. In our case, this is useful when separating the papillary muscles from the blood pool. Malladi et al. [16,17] showed how level-set algorithms could be applied for enhancement and shape recovery in medical images. An extension of Malladi's work, performed by Niessen et al. [18] uses a more diffusive propagation term to increase the influence of the stopping term.

Zeng et al. [19] first introduced the idea of coupled level sets for segmentation of the cortex of the brain. The coupled level set can use the constant thickness or distance between the level-sets as a constraint to avoid spilling or over segmentation. The ideas introduced by Zeng were extended by Paragios [20] who applied a similar coupling constraint for the segmentation of the myocardium of the heart.

Leventon et al. [21] introduced a priori knowledge by building an a priori model that was embedded in a level set formalisation and evaluating its modes of variation using PCA analysis.

Variational approaches to segmentation using a two class or more partitioning within the image have been investigated. Chen and Vese [22] implemented the Mumford and Shah [23] functional in a level-set framework. Probabilistic approaches have also been investigated, where curve propagation is controlled using the probabilistic membership of signal intensity to the expected prior intensity values of the structure to be

segmented. Paragios [24] describes a multiple class probability problem which uses a priori intensity information about the structures (left ventricle blood pool and myocardium) to be segmented. Curve evolution is then performed by minimizing the energy using this a priori intensity based information, boundary information and a collection of shape based model constructed from prior segmentations. While this algorithm performs well in homogenous regions, the nature of MRI image acquisition implies that the signal intensity is subject to variation through the dataset and, therefore, partitioning the data using prior signal intensity information may not be appropriate.

To address the problems faced by probabilistic partitioning methods, we introduce a novel formulation that performs a gradient-based coupled level-set segmentation of the left ventricle myocardium. We increase robustness in the segmentation in areas of low edge strength by incorporating both gradient and texture information. This segmentation is supervised by incorporating a priori knowledge into the evolution and applying this information in a global sense to avoid leaking and selecting false local minima. The a priori model is a probability function derived from manually segmented heart images which biases results towards a training set. Due to the low signal-to-noise ratio (SNR) present in MRI scans, region based information is included in the deformation, which gives improved robustness in the segmentation of a wide variation of cardiac morphologies. Analysis of point-to-curve errors, reproducibility plots and correlation results are provided on data-sets of the heart and compared against manual delineation.

2. Method

A level-set segmentation is performed to robustly segment the myocardium of the left ventricle of the heart. Level-set segmentation involves a deformable curve or surface evolving under gradient information and the intrinsic curvature. To overcome limitations with gradient based stopping terms, we introduce a region-based term to the stopping function to increase robustness. To further control the evolution, two additional features have been applied. Firstly, a coupled level-set is introduced, representing the endo- and epicardium boundaries of the left ventricle. These two level-sets interact with each other through the evolution using a coupling function. This prohibits the endocardium boundary joining with the epicardium boundary and also restricts the epicardium boundary spilling where there is no gradient information available. The second feature to be added to the evolution is a priori information, obtained from manual segmentations of the endo- and epicardium boundaries. This controls the evolution to bias manually defined shapes of the left ventricle muscle.

2.1. Level-set formulation background

The fundamental objective behind level-sets is to track a closed interface $\Gamma(t)$, for which $\Gamma(t): [0, \infty] \rightarrow R^N$, as it evolves in the data space. The interface is represented by a curve in 2D and a surface in 3D or the set of points that are on the boundaries of the region of interest Ω . Caselles et al. [14] formalised

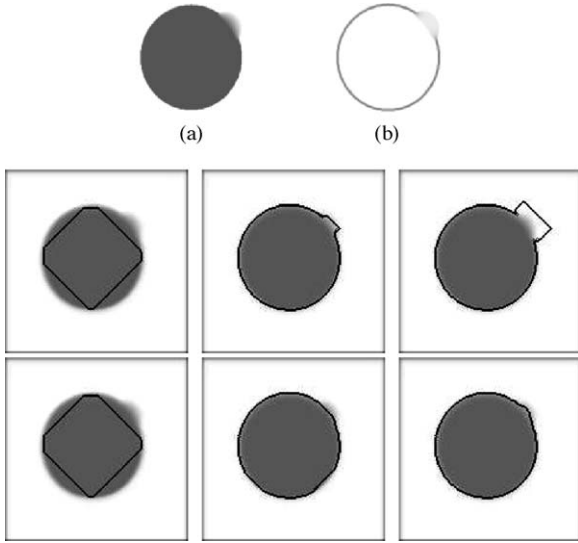


Fig. 1. The original phantom image with a diffused segment (a) and Sobel edge image (b). The second row shows the evolution with the existing $g = 1/(1 + \nabla I)$ at iteration 0, 25 and 50 while the third row shows the evolution with our proposed approach where $g = 1/(1 + \nabla II_{\sigma})$ iteration 0, 25 and 50.

the minimization of the classic energy function used in snake evolution for the extension to level-set theory.

$$\min \int g(|\nabla I(\Gamma(s))|, I_{\sigma})|\Gamma'(s)|ds \quad (1)$$

We reformulate the stopping term to include the gradient (∇I) and region changes (I_{σ}) at that position. This improves segmentation by enforcing homogeneity within the region Ω being segmented and is illustrated in Figs. 1 and 2. In Eq. 1, ∇I is the gradient value measured across a six connected 3D neighborhood. I_{σ} is a measure of the change in texture and is calculated by firstly measuring the mean and variance of the voxels chosen

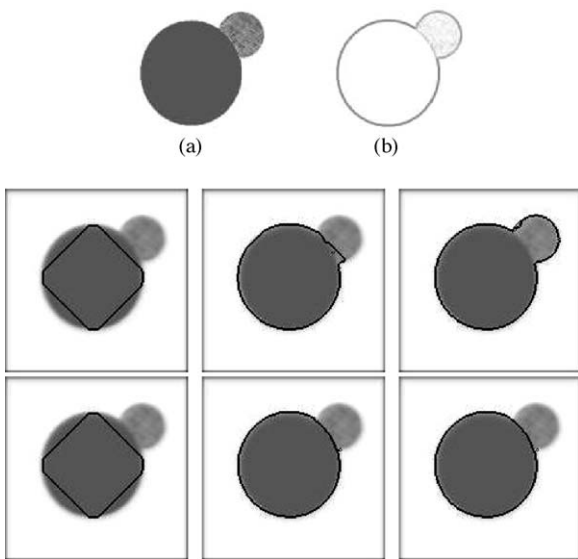


Fig. 2. The original phantom image with a close region (a) and Sobel edge image (b). The second row shows the evolution with the existing $g = 1/(1 + \nabla I)$ at iteration 0, 25 and 50 while the third row shows the evolution with our proposed approach where $g = 1/(1 + \nabla II_{\sigma})$ iteration 0, 25 and 50.

during the initialisation stage.

$$g = \frac{1}{1 + (\nabla I/I_{\sigma})} \quad (2)$$

Level-set theory aims to exchange the Lagrangian formalisation and replace it with Eulerian, initial valued partial differential equation evolution. From [14] it can be shown that the Euler–Lagrange gives a minimizing curve that is of the form.

$$\frac{d}{dt} \Gamma(s) = g(|\nabla I|)\kappa \vec{n} - (\nabla g \cdot \vec{n})\vec{n} \quad (3)$$

The term $\nabla g \cdot \vec{n}$ is a naturally accuring attraction force vector normal to the surface and κ is the curvature term. By representing the boundary as the zero level set instance of a higher dimensional function ϕ , the effects of curvature can be easily incorporated. ϕ is represented by the continuous Lipschitz function $\phi(s, t = 0) = \pm d$, where d is the signed distance from position s to the initial interface Γ_0 . The Lipschitz condition implies that the function has a bounded first derivative. The distance is given a positive sign outside the initial boundary ($D\Omega$), a negative sign inside the boundary ($\Omega \setminus \partial\Omega$) and zero on the boundary ($\partial\Omega$).

$$\phi(s) = \begin{cases} -d & \forall s \in \Omega \setminus \partial\Omega \\ 0 & \forall s \in \partial\Omega \\ +d & \forall s \in R^n \setminus \Omega \end{cases} \quad (4)$$

From this definition of ϕ , intrinsic properties of the front can be easily determined, like the normal $\vec{n} = \pm(\nabla\phi/|\nabla\phi|)$ and the curvature $\kappa = \nabla(\nabla\phi/|\nabla\phi|)$.

In the segmentation scheme we would like to add a non-zero internal advection or ballooning force, c , to the evolution, to evolve the either outward ($c = 1$) or inward ($c = -1$). β and ϵ are independent user defined parameters controlling the effects of attraction to gradients and curvature, respectively.

$$\frac{\partial\phi}{\partial t} = g(|\nabla I|)(c + \epsilon\kappa)|\nabla\phi| + \beta(\nabla g \cdot \nabla\phi) \quad (5)$$

2.1.1. Determination of the stopping term

To illustrate the improved performance of the advanced stopping term, the following phantom images were created and tested. Two situations are described, the first where the edge strength between two regions were diffused to reduce the gradient information (see Fig. 1) and the second case where the grayscale difference between two regions was low (see Fig. 2). The stopping term, as defined in Eq. (2), uses a combination of the gradient and change in texture. The change in texture (I_{σ}) is calculated after the initialisation using the fast marching algorithm described in Section 2.4. Within the initialised region the mean μ and variance σ of the voxels are calculated. From these values, a Gaussian is constructed and the $I_{\sigma}(s)$ is calculated as,

$$I_{\sigma}(s) = \frac{1}{2\pi\sigma^2} e^{-(x-\mu)^2/2\sigma^2} \quad (6)$$

where x is the value of the voxel at each position s in the $3 \times 3 \times 3$ neighbourhood. The value of I_{σ} is normalised between 0 and 1. The use of a Gaussian distribution is proposed as a measure of probability that the evolving contour incorporates voxels that

belong to the structure and has been previously used to model tissue response in MRI [25,26].

The user-defined parameters ε and β represent the influence of the curvature and attraction to gradient on the evolving boundary. In the following tests, we want to evaluate the influence of the improved stopping term, so the value of ε is given less significance to reduce the influence of curvature on the evolution. In the segmentation of the left-ventricle boundaries, the value of ε is given a higher significance as we know the boundaries approximate circles. Similarly, β controls the attraction of the level-set boundary to gradients that are normal to the curve. Again, this value is given a reduced weighting in the proceeding tests. The results shown in Figs. 1 and 2 demonstrate the improved robustness against boundary leaking between regions.

2.2. Coupling force

To further control the level-set evolution we employ a coupling function between two level-sets. The coupling adds an extra constraint by introducing a second level-set that is dependent on the first and coupling the level-sets with an inhibitor function, which allows the curve to change direction of growth. This is achieved without any extra computational expense as the distance between any point to the level-set boundary is the value of ϕ at that point, see Eq. (4). The piecewise inhibitor function, which is used as the interaction between the two level-sets, is defined below, where d is the preferred distance between the endo- and epicardium surfaces and w controls the slope between inward and outward growth. The result $\eta_2(\phi_1)$ changes value from +1 to -1, which changes the direction of the evolution for ϕ_2 between inwards and outwards. In practice the values of d and w are taken from the scaled a priori model.

$$\eta_2(\phi_1) = \begin{cases} -1 & \text{for } \phi_1(s) < -d - w \\ \sqrt[3]{\frac{\phi_1(s) - d}{w}} & \text{for } -d - w < \phi_1(s) < d + w \\ 1 & \text{for } \phi_1(s) > d + w \end{cases} \quad (7)$$

For this segmentation scheme, it is assumed that the gradient between the blood pool and the endocardium boundary is significantly high to halt the evolution of the level-set, also it is known that in some cases there is little or no gradient information between the epicardium boundary and the lungs or liver (Fig. 3).

Therefore, the level-set segmenting the epicardium boundary is controlled by the endocardium level-set using the inhibitor function described.

2.3. Introducing priors

A priori information is incorporated with a probability density function (PDF), which is defined as $P(s) = \int f(s) ds$. The model is built from a set of hand segmented boundaries, a probability density function is created of both the endocardium and epicardium boundaries that are then interpolated in the z

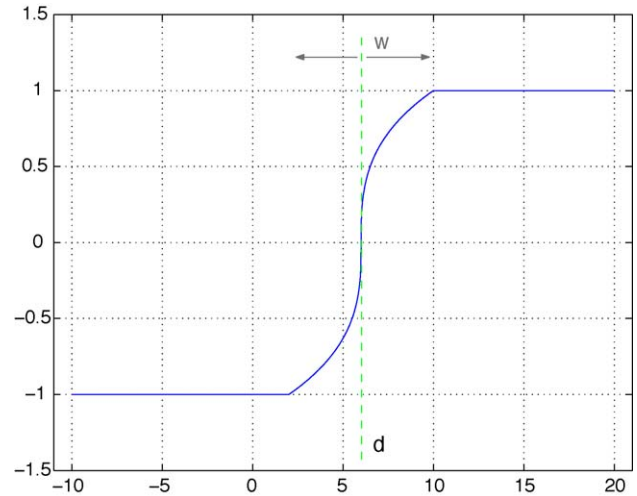


Fig. 3. Graph of the inhibitor function where the values of $d=6$ and $w=4$. The value d represents the nominal distance between the endo-cardium and epicardium boundary and w represents the transition width. Both these values may be obtained from the PDF.

direction using linear interpolation, scaled and aligned in the xy direction.

The PDF is constructed by aligning the binary manually segmented boundary images and summing the boundary elements. This is done for both the endocardium boundary and the epicardium boundary. It is incorporated into the evolution in a global context, after each iteration the value ρ_t is evaluated as,

$$\rho_t = \sum \phi(t)_s \times P_s \quad (8)$$

where $\phi(t)_s$ is the value of ϕ at time t at the position s and P_s is the probability density at position s .

In order to obtain the full evolution equation for the level-set we have to incorporate both the coupling function and the a priori knowledge into Eq. (5). Firstly, the output from the coupling function is either 1 or -1 and we want it to change the direction of the curve evolution. From Eq. (5) we can see that the advection force defines the direction of the evolution, therefore, we incorporate the coupling function by multiplying it with the advection force c . The a priori is designed to disregard inappropriate gradients and give significance only to gradients that are situated close to previously manually segmented boundaries. For this reason, we incorporate the a priori information in the attraction term from Eq. (5). Thus, the complete evolution for the coupled level-set is defined as,

$$\phi_{t+1} = \phi_t + g(|\nabla I|)(c\eta + \varepsilon\kappa)|\nabla\phi| + \frac{\beta}{1 + \tilde{\rho}_t}(\nabla g \cdot \nabla\phi) \quad (9)$$

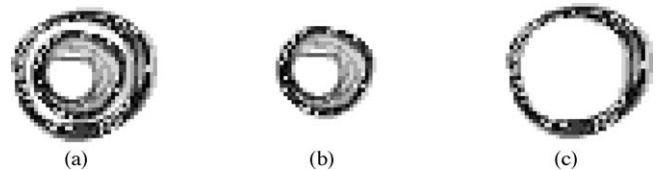


Fig. 4. Images show the probability density functions from a priori hand segmented images. (a) Shows the combined contours while (b) and (c) show the endo- and epicardium boundaries, respectively. Darker gray tone defines a higher probability of the boundaries.

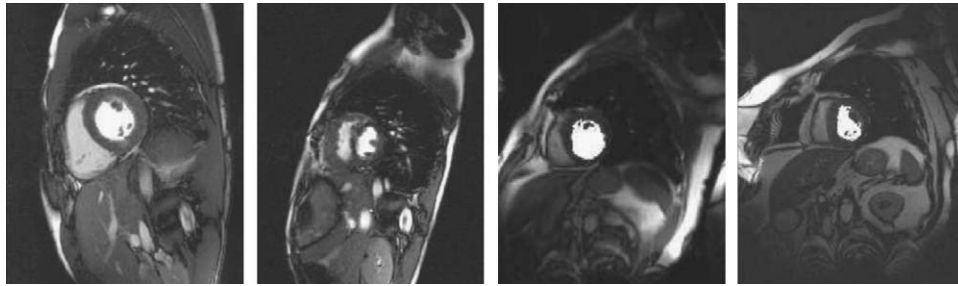


Fig. 5. Results show the initialisation (marked in white) from a seeded fast marching algorithm. The method was applied to perform a robust initial estimate of left ventricle cavity of the heart on four separate datasets displaying a high variability of left ventricle shape.

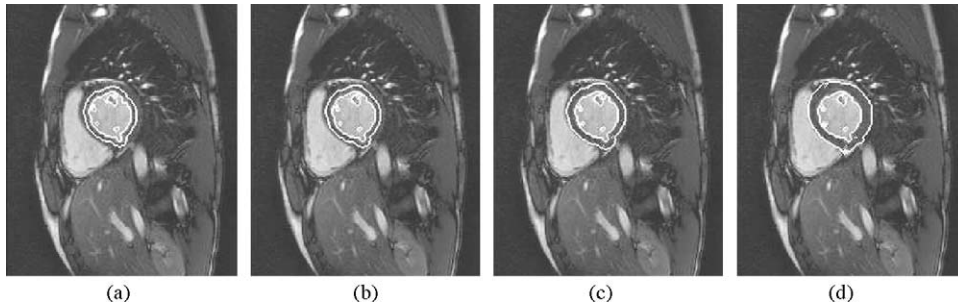


Fig. 6. The images above show evolution of the front at four different iterations (a) iteration=0, (b) iteration=5, (c) iteration=10 and (d) iteration=15.

where η is the result of the coupling function between the level-sets and is defined in Eq. (7) and ρ_t is the a priori knowledge and is defined in Eq. (8).

2.4. Initialisation

To counteract the ‘myopic’ characteristics of these deformable models, the initialisation process is very influential and is performed as follows. Firstly, it is known that the endocardium boundary can be characterised by the high contrast between the blood and the heart muscle in standard (TruFISP) cine imaging of the heart (Fig. 4). This characteristic is used when a fast marching algorithm is applied to find a fast efficient initialisation for the blood following the manual insertion of a seed point. The fast marching approach is driven by a force $F_s = e^{-\alpha \nabla I_s}$, which has a diffusive effect aimed at halting the fronts progress at regions of high gradient. This fast marching approach falls short of the gradient defining the transition from blood to muscle. Therefore, the contour found by the fast

marching algorithm is used as the initial curve of the level-set algorithm to find the endocardium boundary. The results from the fast marching initialisation are illustrated in Fig. 5.

To find the epicardial boundary the endocardium initialisation is dilated slightly and the inner gradients are masked. Both curves are given a positive advection force to propagate outwards. It is known that both the endo- and epicardium boundaries of the left ventricle are approximately circular, therefore the ϵ is given a high significance in the evolution. High curvature constraints, the distance inhibitor and the a priori constraints all act to limit the epicardium front from joining the inner front or spilling in areas of low gradient, like the liver or the lungs (Figs. 6 and 7).

3. Results

In order to assess the performance of the segmentation, the results were compared against those obtained by manual segmentation of the endo- and epicardium boundaries. The algo-

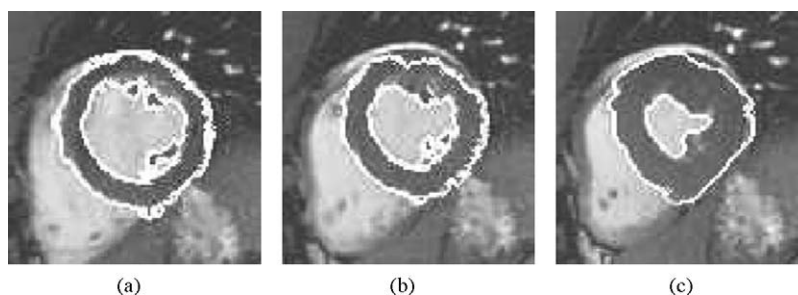


Fig. 7. Segmentation results of the same slice at three separate phases through the hearts cycle: (a) end-diastolic, (b) mid-diastolic and (c) end-systolic.

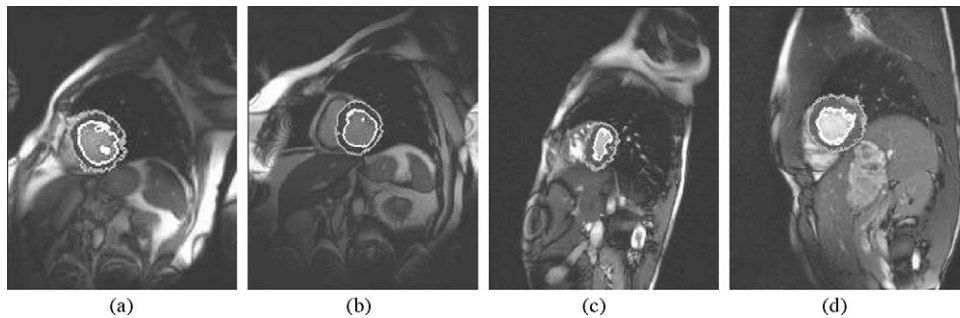


Fig. 8. The images above show the segmentation using our method on the four previously unseen datasets.

Table 1
Point-to-curve errors between manually segmented data and our method

	Point-to-curve error	
	Endocardium	Epicardium
Average	0.477	1.149
Root mean square	0.839	1.649
Standard deviation	0.683	1.157

rithm is applied to four unseen datasets (see Fig. 8) with a high variation between datasets to assess the robustness when using the coupling function and the a priori model. The datasets have a variation in pixel spacing (1.1–2.3 mm/pixel) so all error measurements are given in pixels. Table 1 represents the average, root mean square and variation of the point to curve error for both the endocardium boundary and the epicardium boundary.

The results were then assessed in 2D using the areas enclosed in the endo- and epicardium boundaries (see Figs. 9 and 10).

The results are displayed in linear regression plots and in Bland–Altman [27] plots to assess reproducibility. In the Bland–Altman plots, the x -axis is the manually determined area and the y -axis represents the difference between the manual and automatically determined area. The high gradient information present between the myocardium and the blood pools plays a crucial role in the accurate segmentation of the endocardium which yields a correlation factor of 0.86. To maintain the generality of this approach the parameters were unchanged for all datasets assessed. The correlation factor for the epicardium areas regression is 0.85. The higher than expected error illustrated in the Bland–Altman plots for Figs. 9 and 10 can be explained with the high variation of the datasets, in particular see Fig. 8(c). To illustrate the influence of this dataset on the results, the dataset was removed and the results evaluated again. With this dataset removed (11% of the total number of images) the regression values increase to 0.89 and 0.87 for the endocardium and epicardium boundaries, respectively.

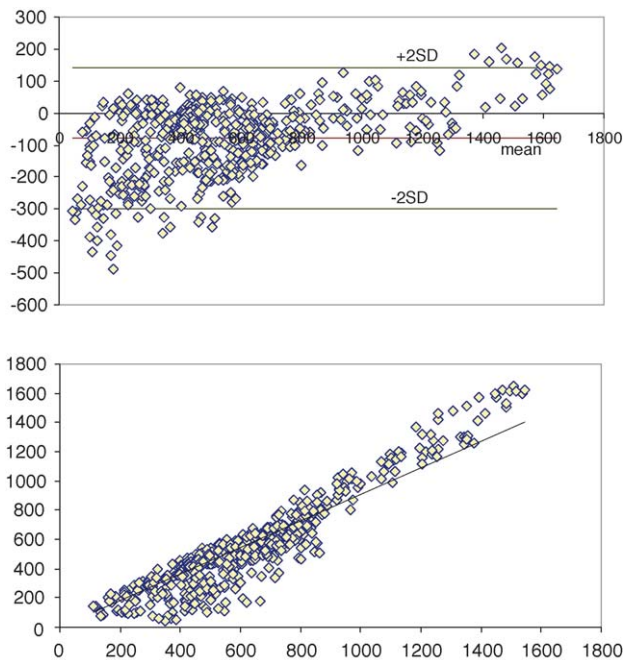


Fig. 9. The Bland–Altman plot and linear plot of the automatic segmentation against the manual segmentation for the endocardium for all datasets shown in Fig. 8.

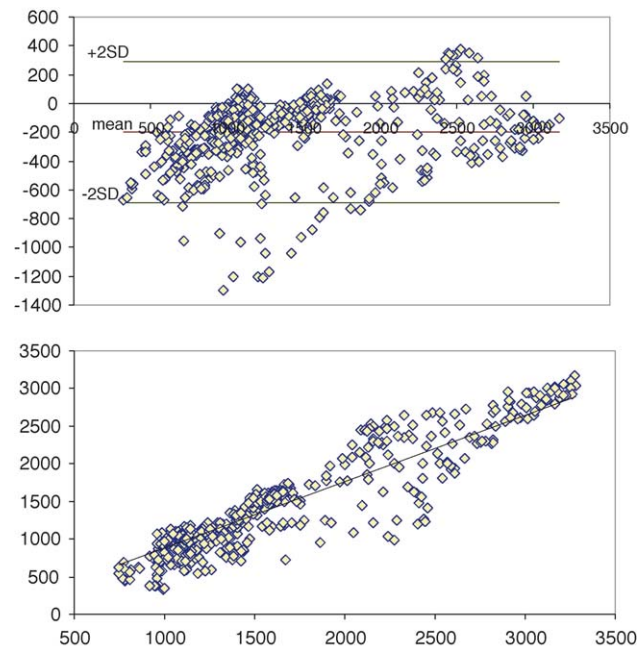


Fig. 10. The Bland–Altman plot and linear plot of the automatic segmentation against the manual segmentation for the epicardium for all datasets shown in Fig. 8.

Computationally, the level-set is less efficient when compared to point evolution methods like snakes. Our implementation performs computation in a narrow-band to improve efficiency. The construction and re-initialisation of this narrow-band can be optimised, as in Chen et al. [28]. Our algorithm has been developed on a Pentium IV 1.4 GHz PC, with 512 MB RAM running Windows 2000. The algorithm has not being optimised for computational speed and currently, using the datasets shown, the iterative steps run at 0.4 s to grow the fast marching algorithm over 3000 voxels. The level-set iterates in 10–40 s within a narrow band of 10 voxels, depending on the number of points in the boundaries.

Kaus et al. [4] report a mean error of 2.45 ± 0.75 mm for the end-diastolic phase and 2.84 ± 1.05 mm for end-systolic phase using a deformable model technique, while our method returns an overall mean error of 0.76 ± 1.09 mm for the endocardium and 1.83 ± 1.85 mm for the epicardium for all phases of the cardiac cycle. The improved performance returned by our algorithm is generated by the improved stopping term and the unique coupling function that is aided by the implicit nature of the level-set function ϕ .

4. Conclusions and future work

The qualitative and quantitative results presented in this paper proves the validity of our coupled level-set method for cardiac myocardium segmentation. This paper describes a novel level-set segmentation where the evolution of the coupled fronts are dependent on both a coupling function and a model trained on real data. An improved stopping term is introduced that is dependent on both gradient and region information.

Positive aspects of the method include the accurate segmentation of the boundaries of the heart. Such a boundary based segmentation can give more accurate results than model fitting approaches, especially in the presence of pathologies. Improved robustness is achieved by using a coupled level-set approach. The method is constrained to limit over segmentation using both a distance inhibitor and is predisposed to replicate expert manual segmentations.

Using the probabilities obtained from the PDF of the training set, our method addresses the limitation of model-based approaches where there is a tradeoff between accuracy and generality. In these approaches, strengthening the a priori's influence on the evolution may result in loss of segmentation detail, patient abnormalities, muscle dysfunction, etc. Investigating ways of improving accuracy without removing generality are part of our plans to further develop the method.

References

- [1] Lelieveldt BPF, van der Geest RJ, Lamb HJ, Kayser HWM, Reiber JHC. Automated observer-independent acquisition of cardiac short-axis MR images: a pilot study. *Radiology* 2001;221(2):537–42.
- [2] Pednekar A, Kakadiaris IA, Kurkure U. Adaptive fuzzy connectedness-based medical image segmentation. In: *Indian Conference on Computer Vision, Graphics and Image Processing* 2002. Ahmedabad, India, December 2002.
- [3] Kass M, Witkin A, Terzopoulos D. Snakes: active contour models. *Int J Comput Vis* 1988;1(4):321–31.
- [4] Kaus M, von Berg J, Niessen WJ, Pekar V. Automated segmentation of the left ventricle in cardiac mri. *Med Image Anal* 2004;8:245–54.
- [5] Cootes TF, Edwards GJ, Taylor CJ. Active appearance models. *Lect Notes Comput Sci* 1998;1407:484–98.
- [6] Hamarneh G, Gustavsson T. Combining snakes and active appearance shape models for segmenting the human left ventricle in echocardiographic images. *IEEE Comput Cardiol* 2000;27:115–8.
- [7] Rogers M, Graham J. Robust active shape model search. In: *Proceedings of the 7th European Conference on Computer Vision*, May 2002, p. 517–30.
- [8] Stegmann MB, Larsson HBW. Motion-compensation of cardiac perfusion MRI using a statistical texture ensemble. In: *Functional Imaging and Modelling of the Heart (FIMH'03)*, Lyon, France, June 2003, p. 151–61.
- [9] Mitchell SC, Lelieveldt BPF, van der Geest RJ, Bosch HG, Reiber JHC, Sonka M. Multistage hybrid active appearance model matching: segmentation of left ventricles in cardiac MR images. *IEEE Trans Med Imaging* 2001;20(5):415–23.
- [10] Bosch JG, Mitchell SC, Lelieveldt BPF, Nijland F, Kamp O, Sonka M, Reiber JHC. Automatic segmentation of echocardiographic sequences by active appearance motion models. *IEEE Trans Med Imaging* 2002;21(11).
- [11] Osher S, Sethian JA. Fronts propagating with curvature-dependent speed: algorithms based on Hamilton–Jacobi formulations. *J Comput Phys* 1988;79:12–49.
- [12] Sethian JA. An analysis of flame propagation. Ph.D. thesis, University of California, Department of Mathematics, University of California, Berkeley, CA, USA, 1982.
- [13] Sethian JA. A marching level set method for monotonically advancing fronts. In: *Proceedings of the National Academy of Sciences*, vol. 93, 1996.
- [14] Caselles V, Kimmel R, Sapiro G. Geodesic active contours. *Int J Comput Vis* 1997;22(1):61–79.
- [15] Caselles V, Catté F, Coll T, Dibos F. A geometric model for active contours in image processing. *Numerische Mathematik* 1993;66(1): 1–31.
- [16] Malladi R, Sethian JA, Vermuri BC. Shape modeling with front propagation: a level set approach. *IEEE Trans Pattern Anal Machine Intell* 1995;17:158–75.
- [17] Malladi R, Sethian JA. Level set methods for curvature flow, image enhancement, and shape recovery in medical images. In: *Proceedings of Conference on Visualization and Mathematics*, Berlin, Germany, June 1997.
- [18] Niessen WJ, ter Haar Romeny BM, Viergever MA. Geodesic deformable models for medical image analysis. *Trans Med Imaging* 1998;17(4):634–42.
- [19] Zeng X, Staib LH, Schultz RT, Duncan JS. Segmentation and measurement of the cortex from 3D MR images. In: *Medical Image Computing and Computer Assisted Intervention, MICCAI*, October 1998.
- [20] Paragios N. A variational approach for the segmentation of the left ventricle in cardiac image analysis. *Int J Comput Vis* 2002;50(3):345–62.
- [21] Leventon ME, Grimson WEL, Faugeras O. Statistical shape influence in geodesic active contours. In: *Proceedings of Computer Vision and Pattern Recognition*, 2000.
- [22] Chan T, Vese L. Active contours without edges. *IEEE Trans Image Process* 2001;10(2):266–77.
- [23] Mumford D, Shah J. Optimal approximations by piecewise smooth functions and associated variational problems. *Comm Pure Appl Math* 1989;42(5):577–85.
- [24] Paragios N. A level set approach for shape-driven segmentation and tracking of the left ventricle. *IEEE Trans Med Imaging* 2003;22(6):773–6.
- [25] Laidlaw DH, Fleischer KW, Barr AH. Partial-volume bayesian classification of material mixtures in mr volume data using voxel histograms. *IEEE Trans Med Imaging* 1998;17(1):74–86.

- [26] Khalighi M, Soltanian-Zadeh H, Lucas C. Unsupervised mri segmentation with spatial connectivity. In: Proceedings of the SPIE International Symposium on Medical Imaging, February 2002.
- [27] Bland JM, Altman DG. Statistical methods for assessing agreement between two methods of clinical measurements. *Lancet* 1986;1(8476):307–10.
- [28] Chen Q, Zhou Z, Qu Y, Heng PA, Xia D. Level set based auto segmentation of the tagged left ventricle mr images. In: Proceedings of Medicine Meets Virtual Reality 12, vol. 12, Newport Beach, CA, USA, 2004, p. 63–65.

Michael Lynch graduated with a B.Eng. (Hons) degree in Mechatronic Engineering from Dublin City University, Dublin, Ireland in 2002. He obtained his PhD for work on multidimensional analysis in cardiac MRI performed within the Vision Systems Group in Dublin City University. His research interests include image processing with particular emphasis on medical image analysis.

Dr. Lynch currently holds a position of research scientist with Siemens Corporate Research in Erlangen Germany working on a European funded project, where he will work within a large European-wide collaboration focussing on data processing and interpretation in paediatric health care.

Ovidiu Ghita received his BE and ME degrees in Electrical Engineering from Transilvania University Brasov, Romania. From 1994 to 1996 he was an Assistant Lecturer in the Department of Electrical Engineering at Transilvania University. Since then he has been a member of the Vision Systems Group at Dublin City University (DCU) during which time he received his PhD for work in the area of robotic vision (2000). Currently, he holds a position of Postdoctoral Research Assistant in the Vision Systems Group at DCU.

Dr. Ghita has authored and co-authored more than 50 peer-reviewed research papers in areas of machine vision, range acquisition, instrumentation and medical imaging.

Paul F. Whelan received his B.Eng. (Hons) degree in Electronic Engineering from the National Institute for Higher Education Dublin, a M.Eng. degree from the University of Limerick, and his PhD (Computer Science) from the University of Wales Cardiff (UK). During the period 1985–1990 he was employed by Industrial and Scientific Imaging Ltd and later by Westinghouse (WESL), where he was involved in the research and development of industrial vision systems. He was appointed to the School of Electronic Engineering, Dublin City University (DCU) in 1990 and is currently a full Professor and holds a Personal Chair. Prof. Whelan set up the Vision Systems Laboratory and its associated Vision Systems Group in 1990 and currently serves as its director, as well as publishing over 100 peer reviewed papers. Prof. Whelan has co-authored two monographs namely “Intelligent Vision Systems for Industry” (1997-Springer) and “Machine Vision Algorithms in Java: Techniques and Implementation” (2000-Springer, reprinted in 2001). He has also co-edited three books including “Selected Papers on Industrial Machine Vision Systems” (1994-SPIE). His research interests include image segmentation, and its associated quantitative analysis (specifically mathematical morphology, colour-texture analysis) with applications in computer/machine vision and medical imaging (specifically computer aided detection and diagnosis focusing on translational research). He is a senior member of the IEEE, a Chartered Engineer and a member of the IET and IAPR. Prof. Whelan is a member of the governing board of the International Association for Pattern Recognition (IAPR) and the current President of the Irish Pattern Recognition and Classification Society (IPRCS).